Journal of Applied Sciences

ISSN 1812-5654

science alert

ANSInet
an open access publisher
http://ansinet.com

Journal of Applied Sciences 5 (5): 1452-1460, 2005
ISSN 1812-5654

Comparison of Boundary Mapping Efficiency of Gradient Vector Flow Active Contours and their Variants on Chromosome Spread Images

[1]A. Prabhu Britto and [2]G. Ravindran
[1]Center for Medical Electronics, Department of Electronics and Communication Engineering
[2]Faculty of Information and Communication Engineering, Anna University, Chennai 600 025, India

Abstract: This study compares the boundary mapping efficiency of curve evolution method on chromosome spread images. The curve evolution methods chosen for comparison gradient vector flow active contours, generalized gradient vector flow active contours, discrete cosine transform based gradient vector flow active contours and discrete cosine transform based generalized gradient vector flow active contours. Chromosome spread images were characterized by chromosome images with variable shape and image properties. Experimental results showed that gradient vector flow active contours and its variants were successful boundary mapping tools for chromosome spread images. The result of this comparison was expected to yield a very efficient boundary mapping scheme for boundary mapping chromosome spread images.

Key words: Active contours, chromosome spread images, boundary mapping, gradient vector flow

INTRODUCTION

This study compares the boundary mapping efficiency of curve evolution method on chromosome spread images. The variations in shape and other image properties in chromosome spread images demand a highly efficient technique for boundary mapping. Active contours show much promise for the task of boundary mapping in chromosome spread images. Concentration is focused on gradient vector flow active contours as they are successful in boundary mapping chromosome spread images[1]. The main advantage of active contour models is the ability to generate closed parametric curves from images and incorporation of a smoothness constraint that provides robustness to noise and spurious edges.

ACTIVE CONTOUR MODELS

Active contours also called as Snakes or Deformable curves, first proposed by Kass *et al.*[2] are energy-minimizing contours that apply information about the boundaries as part of an optimization procedure. They are generally initialized around the object of interest by automatic or manual process. The contour then deforms itself iteratively from its initial position in conformity with nearest dominant edge feature by minimizing the energy composed of the internal and external forces, thus making the model active. The energy minimization process can be viewed as a dynamic problem where the active contour model is governed by the laws of elasticity and lagrangian dynamics[3] and the model evolves until equilibrium of all forces is reached.

FORMULATION OF ACTIVE CONTOUR MODELS

An active contour model can be represented by a curve c, as a function of its arc length τ,

$$c(\tau) = \begin{pmatrix} x(\tau) \\ y(\tau) \end{pmatrix} \quad (1)$$

with $\tau = [0...1]$. To define a closed curve c (0) is set to equal c(1). A discrete model can be expressed as an ordered set of n vertices $v_i = (x_i, y_i)^T$ with $v = (v_1, \ldots, v_n)$. The large number of vertices required to achieve accuracy could lead to high computational complexity and numerical instability[3]. Mathematically, an active contour model can be defined in discrete form as a curve $x(s) = [x(s), y(s)], s\varepsilon[0,1]$ that moves through the spatial domain of an image to minimize the energy functional

$$E = \int_0^1 \frac{1}{2}(\alpha|x'(s)|^2 + \beta|x''(s)|^2) + E_{ext}(x(s))ds \quad (2)$$

Where, α and β are weighting parameters that control the active contour's tension and rigidity, respectively[4]. The first order derivative discourages stretching and the second order derivative discourages bending. α and β

Corresponding Author: A. Prabhu Britto, Center for Medical Electronics,
Department of Electronics and Communication Engineering,
Anna University, Chennai 600025, India

govern the effect of the derivatives on the snake. The external energy function E_{ext} is derived from the image so that it takes on its smaller values at the features of interest such as boundaries and guides the active contour towards the boundaries. The external energy is defined by:

$$E_{ext} = \kappa\left|G_\sigma(x,y)\times I(x,y)\right| \quad (3)$$

Where, $G_\sigma(x,y)$ is a two-dimensional gaussian function with standard deviation σ, I(x,y) represents the image and κ is the external force weight. This external energy is specified for a line drawing (black on white) and positive κ is used. A motivation for applying some Gaussian filtering to the underlying image is to reduce noise.

An active contour that minimizes E must satisfy the Euler equation:

$$ax''(s) - \beta x''''(s) - \nabla E_{ext} = 0 \quad (4)$$

Where, $F_{int} = ax''(s) - \beta x''''(s)$ and $F_{ext} = -\nabla E_{ext}$ comprise the components of a force balance equation such that:

$$F_{int} + F_{ext} = 0 \quad (5)$$

The internal force F_{int} discourages stretching and bending while the external potential force F_{ext} drives the active contour towards the desired image boundary. Equation 4 is solved by making the active contour dynamic by treating x as a function of time t as well as s. Then the partial derivative of x with respect to t is then set equal to the left hand side of Eq. 4 as follows:

$$x_t(s,t) = ax''(s,t) - \beta x''''(s,t) - \nabla E_{ext} \quad (6)$$

A solution to Eq. 6 can be obtained by discretizing the equation and solving the discrete system iteratively[2]. When the solution x (s,t) stabilizes, the term x_t (s,t) vanishes and a solution of Eq. 4 is achieved.

Traditional active contour models suffer from a few drawbacks. Boundary concavities leave the contour split across the boundary. Capture range is also limited. Methods suggested to overcome these difficulties, namely multiresolution methods[5], pressure forces ,[6] distance potentials[7], control points ,[8] domain adaptivity[9], directional attractions[10] and solenoidal fields[11], however solved one problem but introduced new ones[12]. Hence, this new class of external fields called Gradient Vector Flow fields[12,13] was suggested to overcome the difficulties in traditional active contour models.

GRADIENT VECTOR FLOW (GVF) ACTIVE CONTOURS

Gradient Vector Flow (GVF) active contours use gradient vector flow fields obtained by solving a vector diffusion equation that diffuses the gradient vectors of a gray-level edge map computed from the image. The GVF active contour model cannot be written as the negative gradient of a potential function. Hence it is directly specified from a dynamic force equation. The external forces arising out of GVF fields are non-conservative forces as they cannot be written as gradients of scalar potential functions and they show improved performance compared to traditional energy-minimizing active contours[12,13].

The GVF field points towards the object boundary when very near to the boundary, but varies smoothly over homogeneous image regions extending to the image border. Hence the GVF field can capture an active contour from long range from either side of the object boundary and can force it into the object boundary. The gradient vectors are normal to the boundary surface but by combining Laplacian and Gradient the result is not the normal vectors to the boundary surface. As a result of this, the GVF field yields vectors that point into boundary concavities so that the active contour is driven through the concavities. Information regarding whether the initial contour should expand or contract need not be given to the GVF active contour model. The GVF active contour model has a large capture range. The GVF is very useful when there are boundary gaps, because it preserves the perceptual edge property of active contours[2,13]. Also, the GVF provides for flexible initialization of the initial contour. This GVF field is defined as the equilibrium solution to the following vector diffusion equation[12]:

$$u_t = g(|\nabla f|)\nabla^2 u - h(|\nabla f|)(u - \nabla f) \quad (7a)$$

and

$$u(x,0) = \nabla f(x) \quad (7b)$$

Where, u_t denotes the partial derivative of u(x,t) with respect to t, ∇^2 is the Laplacian operator (applied to each spatial component of u separately) and f is an edge map that has a higher value at the desired object boundary. The functions in g and h control the amount of diffusion in GVF. In Eq. 7, g $(|\nabla f|)\nabla^2 u$ produces a smoothly varying vector field and hence called as the smoothing term, while $h(|\nabla f|)(u-\nabla f)$ encourages the vector field u to be close to ∇f computed from the image data and hence called as the data term. The weighting functions $g(\cdot)$ and $h(\cdot)$ apply to the smoothing and data

terms respectively and they are chosen[13] as $g(|\nabla f|) = \mu$ and $h(|\nabla f| = |\nabla f|^2)$. $g(\cdot)$ is constant here and smoothing occurs everywhere, while $h(\cdot)$ grows larger near strong edges and dominates at boundaries. Hence, the GVF field is defined as the vector field $v^{(x,y)=[u(x,y),v(x,y)]}$ that minimizes the energy functional

$$\varepsilon = \iint \mu(u_x^2 + u_y^2 + v_x^2 + v_y^2) + \left|\nabla f\right|^2 \left|v - \nabla f^2\right| dxa \quad (8)$$

The effect of this variational formulation is that the result is made smooth when there is no data. When the gradient of the edge map is large, it keeps the external field nearly equal to the gradient, but keeps field to be slowly varying in homogeneous regions where the gradient of the edge map is small, i.e., the gradient of an edge map ∇f has vectors point toward the edges, which are normal to the edges at the edges and have magnitudes only in the immediate vicinity of the edges and in homogeneous regions ∇f is nearly zero. μ is a regularization parameter that governs the tradeoff between the first and the second term in the integrand in Eq. 8. The solution of Eq. 8 can be done using the Calculus of Variations and further by treating u and v as functions of time, solving them as generalized diffusion equations[13].

GENERALIZED GRADIENT VECTOR FLOW (GGVF) ACTIVE CONTOURS

In the GVF active contour formulation given by Eq. 7, the term $g(\nabla f)$ is constant and hence smoothing occurs everywhere, while $h(\nabla f)$ grows larger near strong edges, dominating at boundaries. However when there are two edges in close proximity, it manifests as a long, thin indentation along the boundary. This makes the GVF tend to smooth between opposite edges. Hence the GVF loses forces to drive the Active Contour into this region.

Suitable weighting functions are proposed[14] in which $g(\cdot)$ becomes smaller as $h(\cdot)$ becomes larger. Therefore there will be very little smoothing in the proximity of large gradients. Hence the effect vector field will be nearly equal to the gradient of the edge map. There are many ways to specify these pairs of weighting functions, thus making the formulation a Generalized Gradient Vector active contour formulation. The following weighting functions were chosen[14].

$$g(|\nabla f|) = e^{-\left(\frac{|\nabla f|}{\kappa}\right)^2} \quad (9)$$

and

$$h(|\nabla f|) = 1 - g(|\nabla f|) \quad (10)$$

This choice of weighting functions will make the computed GGVF field to conform to the edge map gradient at strong edges, but will vary smoothly away from boundaries. The solution remains the same as discussed in GVF active contours in the preceding paragraphs.

DISCRETE COSINE TRANSFORM (DCT) BASED GVF AND DCT BASED GGVF ACTIVE CONTOURS

The transform of an Image yields more insight into the properties of the image. The Discrete Cosine Transform (DCT) has excellent energy compaction. Hence, the DCT promises better description of the image properties. Therefore, the DCT is embedded into the boundary mapping scheme to obtain better energy compaction. The 2D DCT is defined as:

$$C(u,v) = \alpha(u)\alpha(v)\sum_{x=0}^{N-1}\sum_{y=0}^{N-1} f(x,y)\cos\left[\frac{(2x+1)u\pi}{2N}\right]\cos\left[\frac{(2y+1)v\pi}{2N}\right] \quad (11)$$

The local contrast of the Image at pixel location (k, l) is given by:

$$P(k,l) = \frac{\sum_{t=1}^{2(2n+1)-1} w_t E_t}{d_{00}} \quad (12)$$

where,

$$E_t = \frac{\sum_{u+v=t} |d_{u,v}|}{N} \quad (13)$$

and

$$N = \begin{cases} t+1 & t<2n+1 \\ 2(2n+1)-t & t \geq 2n+1 \end{cases} \quad (14)$$

Here, w_t denotes the weights used to select the DCT coefficients.

The local contrast P(k, l) is then used to generate a DCT contrast enhanced image[15], which is then subject to selective segmentation by the gradient vector flow active contour model using Eq. 2 and the generalized gradient vector flow model using Eq. 8.

MATERIALS AND METHODS

The chromosome spread image (72 pixels per inch resolution) was taken and preprocessed. Insignificant and unnecessary regions in the image were removed interactively. The chromosome of interest was selected by user selection of a few points on the chromosome spread image that formed the vertices of a polygon. On constructing the perimeter of the polygon from the

selection points, seed points for the initial contour were determined automatically by periodically selecting every third pixel along the perimeter of the polygon.

The GVF active contour is governed by the following parameters, namely, σ, μ, α, β and κ. σ determines the gaussian filtering that is applied to the image to generate the external field. Larger value of σ will cause the boundaries to become blurry and distorted and can also cause a shift in the boundary location. However, large values of σ are necessary to increase the capture range of the active contour. μ is a regularization parameter in Eq. 8 and requires a higher value in the presence of noise in the image. α determines the tension of the active contour and β determines the rigidity of the contour. The tension keeps the active contour contracted and the rigidity keeps it smooth. α and β may also take on value zero implying that the influence of the respective tension and rigidity terms in the diffusion equation is low. κ is the external force weight that determines the strength of the external field that is applied. The iterations were set suitably.

RESULTS AND DISCUSSION

The chromosome spread image was subjected to boundary mapping using GVF active contours, GGVF active contours, DCT based GVF active contours and DCT based GGVF active contours.

The results show successful boundary mapping of the chromosome spread images by GVF, GGVF, DCT based GVF and DCT based GGVF active contours (Fig. 1-4). When the result of the boundary mapping by each scheme was compared, it was found that the boundary mapping by DCT based GVF active contours had very less or no indentations compared to the results by the other three schemes.

To substantiate the findings by graphical results, characterization of the parameters was done.

CHARACTERIZATION

A set of 10 samples were taken and characterization of each parameter was done. The outputs were tabulated in ranking order with 1 describing the best quality output and as the quality decreases the rank increases up to rank 97.

Rank 98 was a special case, where the output image was rejected based on quality or the output image was not available due to numerical instability possibly caused due to the greater number of contour points[3]. The tables represent characterization studies for each parameter.

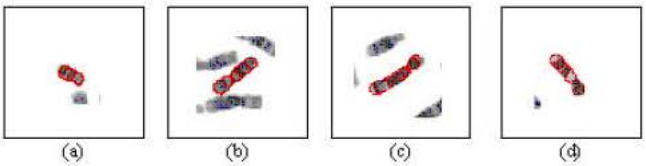

Fig. 1a-d: Chromosome image samples boundary mapped using GVF active contours

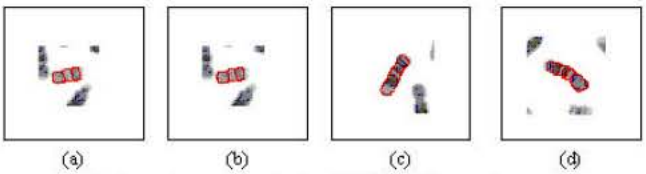

Fig. 2a-d: Chromosome image samples boundary mapped using GGVF active contours

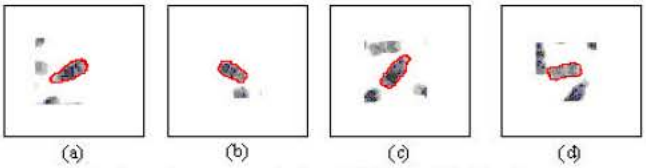

Fig. 3a-d: Chromosome image samples boundary mapped using DCT based GVF active contours

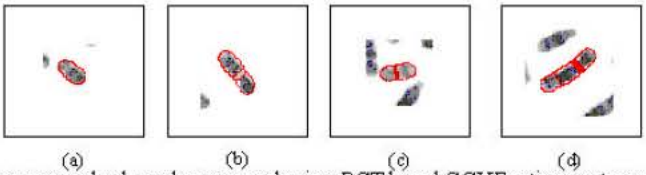

Fig. 4a-d: Chromosome image samples boundary mapped using DCT based GGVF active contours

The statistical median was used to judge the distribution of values for each parameter value for all samples. When the median leans towards the lower values, i.e., towards 1, it indicates that almost 50% of the outputs lean towards 1, which was a good indicator of obtaining majority good outputs on various samples, making that particular parameter value an optimal one.

In each characterization study, a value for the parameter was chosen which gives the maximum good quality outputs for all samples.

Since, each table denotes variation for only one parameter either between the lower and upper limits of the parameter or between the lower and upper limits giving significantly different output, with the other parameters taking a constant value, the best parameter value of that table was the one that gives maximum good quality outputs for all samples or a majority of samples.

Exhaustive study on every parameter treating the other parameters as constants was done. The characterization studies reveal that each parameter sometimes has an optimal range within which it can assume any value thereby giving majority good outputs for all samples.

But for the sake of experimental purposes, only that investigated discrete value of each parameter that gave optimal best output was chosen.

Hence, the characterization had yielded optimal values for the GVF parameters which could be used for similar class of images to obtain good boundary mapping results.

An important point to be noted was that characterization studies had been performed for those parameter values which give either significant output or significant difference in performance between adjacent parameter values.

Those parameter values where there was no significant difference between adjacent parameter values had not been tabulated. Also, those parameter values outside the tabulated range which give no proper results had not been tabulated.

Table 1-20 showed the characterization experimental results in the ranking scale, where 1 denoted the best quality output and the rank increases numerically with decreasing quality up to 98.

In Table 1-20, the parameters act independently on the boundary mapping scheme. In each characterization, the effect of other parameters would also be felt as they assume a definite constant value.

In the course of the characterization study from Table 1-5, optimum values for the respective parameters were chosen and applied as constant in the characterization study of the next parameter in the successive table. In the characterization study shown in Table 5, the values of σ, μ, α and β take on the chosen optimal values and only κ was investigated, thereby yielding a one way variation.

Table 1: Characterization of σ by using GVF active contours

Sample	GVF σ				
No.	0.125	0	0.5	1	1.5
1	45	45	37	45	81
2	50	34	87	11	12
3	49	38	37	33	98
4	48	45	31	31	16
5	50	98	98	98	98
6	48	46	46	58	46
7	98	97	98	98	98
8	90	50	98	98	98
9	86	45	52	98	47
10	77	35	52	82	82
Median	50	45	52	70	82

Table 2: Characterization of μ by using GVF active contours

Sample	GVF μ				
No.	0.005	0	0.1	0.15	0.2
1	29	29	45	39	62
2	29	29	34	33	29
3	34	34	38	45	50
4	31	31	45	32	47
5	98	98	98	90	90
6	37	36	46	62	61
7	98	98	97	98	98
8	91	98	50	97	97
9	29	29	45	47	45
10	45	45	35	35	45
Median	36	35	45	46	56

Table 3: Characterization of α by using GVF active contours

Sample	GVF α						
No.	0.2	0.25	0	0.4	0.4	0.5	1
1	29	87	13	70	13	31	29
2	29	13	13	29	29	29	29
3	29	29	29	75	29	29	98
4	31	31	31	32	31	31	77
5	98	98	98	98	98	98	98
6	98	36	38	36	38	36	55
7	98	98	98	98	98	98	98
8	98	98	98	98	98	98	36
9	31	13	31	13	13	13	29
10	15	15	45	32	29	31	45
Median	31	34	35	53	30	31	50

Table 4: Characterization of β by using GVF active contours

Sample	GVF β					
No.	0	0.2	0.4	0.6	0.8	1
1	13	29	29	31	45	46
2	13	13	77	34	29	46
3	29	45	77	97	29	97
4	31	31	31	31	77	31
5	98	98	98	98	98	98
6	38	36	36	38	42	37
7	98	98	98	98	98	98
8	98	98	98	98	98	98
9	31	29	31	15	31	31
10	45	39	47	47	47	45
Median	35	38	62	43	46	46

Table 5: Characterization of κ by using GVF active contours

Sample	GVF κ											
No.	0.1	0.2	0.25	0.3	0.35	0.4	0.45	0.5	1	0.8	1	1.2
1	97	97	97	29	29	29	46	29	13	29	29	77
2	97	77	77	77	29	29	29	38	13	13	38	13
3	97	13	13	75	34	50	29	11	29	45	74	77
4	97	78	79	80	29	29	29	29	31	98	98	77
5	97	97	97	97	98	98	98	98	98	98	98	98
6	97	97	40	38	37	36	52	46	38	98	98	98
7	97	97	97	98	97	98	98	98	98	98	98	98
8	97	97	97	60	97	54	98	98	98	98	98	98
9	97	78	77	77	77	29	87	46	31	29	29	29
10	97	49	45	45	45	45	46	46	45	13	13	37
Median	97	88	78	76	41	41	49	46	35	72	86	77

Table 6: Characterization of σ by using GGVF active contours

Sample	GGVF σ							
No.	0	0.25	0.5	0.75	1	2	3	4
1	77	77	77	77	13	13	35	39
2	77	13	13	13	13	13	13	33
3	77	78	77	77	29	9	35	37
4	79	77	77	77	29	15	15	39
5	97	97	97	97	97	97	97	97
6	97	97	97	97	97	97	97	97
7	97	97	97	97	97	97	97	97
8	86	86	86	86	86	45	50	42
9	78	78	78	78	13	13	15	29
10	77	77	77	77	77	13	29	29
Median	79	78	78	78	53	14	35	39

Table 7: Characterization of μ by using GGVF active contours

Sample	GGVF μ				
No.	0	0.01	0.05	0.1	1
1	13	13	35	97	97
2	13	13	11	97	97
3	11	9	39	97	97
4	15	15	29	97	97
5	97	97	97	97	97
6	97	97	97	97	97
7	97	97	97	97	97
8	86	45	45	97	97
9	31	31	31	97	97
10	29	29	57	97	97
Median	30	30	42	97	97

Table 8: Characterization of α by using GGVF active contours

	GGVF α		
Sample No.	0	0.5	1
1	13	45	93
2	13	13	13
3	11	97	59
4	15	31	97
5	97	58	97
6	97	86	97
7	97	97	97
8	86	94	97
9	31	31	97
10	29	29	77
Median	30	52	97

Hence, one way analysis of variance on Table 5 is sufficient to test the significance of the entire boundary mapping process done using GVF active contours. A significant outcome from Table 5 would justify that the experimental results of Table 5 were valid, implying that the selected parameter values from Table 1 to 4 used as constants in Table 5 were also valid.

Table 9: Characterization of β by using GGVF active contours

	GGVF β		
Sample No.	0	0.5	1
1	13	23	47
2	13	29	77
3	11	34	29
4	15	31	79
5	97	97	97
6	97	87	86
7	97	87	97
8	86	86	90
9	31	32	80
10	29	29	31
Median	30	33	80

Table 10: Characterization of κ by using GGVF active contours

Sample	GGVF κ						
No.	0.2	0.4	0	0.50	0.60	0.70	0.80
1	97	13	13	13	29	29	39
2	13	13	13	13	13	13	29
3	97	11	11	73	29	29	34
4	97	15	29	70	29	29	46
5	97	97	97	97	54	51	58
6	97	97	97	97	54	64	86
7	97	97	97	97	38	62	97
8	97	86	86	86	94	46	46
9	32	31	29	70	29	29	29
10	97	29	13	29	29	29	29
Median	97	30	29	72	29	29	43

Table 11: Characterization of σ by using DCT based GVF active contours

Sample	DCT GVF σ									
No.	0.05	0.1	0.15	0.2	0	0.5	0.6	0.8	1	1
1	77	77	77	77	77	29	77	29	13	77
2	77	77	77	29	13	13	13	13	29	77
3	97	77	34	29	77	29	78	81	75	78
4	77	77	29	29	31	70	79	79	79	78
5	97	97	97	97	98	98	98	98	98	98
6	86	86	46	38	38	14	38	38	46	78
7	97	97	97	97	98	98	98	98	98	98
8	86	86	86	54	98	98	98	98	98	98
9	77	77	77	77	38	46	15	77	13	79
10	86	77	13	77	46	65	78	13	78	77
Median	86	77	77	66	62	55	78	78	77	78

Table 12: Characterization of μ by using DCT based GVF active contours

Sample	DCT GVF μ					
No.	0.05	0.1	0.09375	0.1125	0.15	0.3
1	23	21	21	23	23	97
2	21	5	23	23	23	97
3	30	29	29	46	50	97
4	23	23	23	40	23	97
5	98	98	98	97	97	97
6	48	40	48	48	46	97
7	98	98	50	50	34	97
8	98	89	62	97	97	97
9	71	86	30	71	71	97
10	23	21	29	71	23	97
Median	39	35	29	49	40	97

Table 13: Characterization of α by using DCT based GVF active contours

Sample No.	DCT GVF α				
	0	0.13	0.25	0.5	1
1	7	23	77	71	77
2	7	30	29	77	30
3	5	67	78	78	67
4	23	23	79	80	80
5	98	98	98	98	97
6	98	48	40	46	87
7	98	98	98	97	97
8	90	86	62	97	94
9	21	23	23	71	27
10	5	7	23	21	71
Median	22	39	70	78	79

Table 14: Characterization of β by using DCT based GVF active contours

Sample No.	DCT GVF β		
	0	0.5	1
1	23	30	71
2	5	21	21
3	5	21	31
4	21	23	71
5	98	98	98
6	98	46	70
7	98	98	98
8	38	94	13
9	23	71	71
10	3	21	30
Median	23	38	71

Table 15: Characterization of κ using DCT based GVF active contours

Sample No.	DCT GVF κ					
	0	0.5	0.6	0.75	0.875	1
1	97	7	5	5	5	5
2	97	3	3	3	1	1
3	97	21	19	21	30	67
4	97	7	7	7	23	71
5	97	98	98	98	98	98
6	97	98	98	98	86	98
7	97	98	98	98	98	98
8	97	86	98	97	98	82
9	97	7	7	23	23	21
10	97	21	5	19	19	21
Median	97	21	13	22	26	69

Table 16: Characterization of σ using DCT based GGVF active contours

Sample No.	DCT GGVF σ				
	0.50	1.00	2.00	4.00	6.00
1	97	77	30	5	77
2	97	77	30	5	29
3	97	30	30	5	57
4	97	71	71	7	32
5	97	86	86	97	58
6	86	86	86	38	48
7	86	86	86	34	86
8	86	86	86	38	38
9	79	79	30	21	31
10	79	29	29	29	29
Median	92	78	50	25	43

Table 17: Characterization of μ using DCT based GGVF active contours

Sample No.	DCT GGVF μ		
	0.005	0.01	0.1
1	21	5	97
2	5	5	97
3	5	5	97
4	23	7	97
5	97	97	97
6	40	38	44
7	50	34	33
8	50	38	33
9	23	21	35
10	23	29	97
Median	23	25	97

Table 18: Characterization of α using DCT based GGVF active contours

Sample No.	DCT GGVF α		
	0.01	0	0.2
1	5	5	21
2	5	5	19
3	5	5	21
4	7	5	16
5	97	97	97
6	38	38	46
7	34	50	50
8	38	38	54
9	21	21	21
10	29	7	21
Median	25	14	21

Table 19: Characterization of β using DCT based GGVF active contours

Sample No.	DCT GGVF β		
	0.02	0.1	0.2
1	5	5	21
2	5	5	21
3	5	5	21
4	5	5	70
5	97	97	97
6	38	48	46
7	50	43	34
8	38	46	86
9	21	7	21
10	7	7	21
Median	14	7	28

Table 20: Characterization of κ using DCT based GGVF active contours

Sample No.	DCT GGVF κ		
	0.4	1	0.6
1	21	5	21
2	5	5	5
3	5	5	21
4	70	5	5
5	97	97	97
6	47	48	46
7	50	43	38
8	54	46	38
9	21	7	30
10	30	7	21
Median	38	7	25

Therefore, a similar one way analysis of variance on Table 10, 15 and 20 was sufficient to test the significance of the boundary mapping process done using GGVF active contours, DCT based GVF active contours and DCT based GGVF active contours, respectively.

At the customary 0.05 significance level, when tested using one way ANOVA, acceptable p-value should be obtained less than 0.05. In Table 5, one way ANOVA test yields a p-value of 1.0003 E-09 for κ using GVF active contours, which rejects the null hypothesis. The very small p-value of 1.0003 E-09 indicates that differences between the column means are highly significant. The probability of this outcome under the null hypothesis was less than 1 in 1,000,000,000. The test therefore strongly supports the alternate hypothesis that one or more of the samples are drawn from populations with different means. This implies that the results did not arise out of mere fluctuations and the results were actually significant. Therefore the experimental results are valid. This justifies that a suitable value of parameter κ could be chosen from Table 5 and that the constant values of parameters σ, μ, α and β used in Table 5 were also valid as these values also had significant influence on the results tabulated in Table 5.

For κ using GGVF active contours (Table 10) and κ using DCT based GVF active contours (Table 15), the p-values from the one way ANOVA test yield 3.2400E-02 and 7.1708E-08, respectively, which establish that the experimental results are valid. The characterization for κ using DCT based GGVF active contours (Table 20) yields a p-value of 6.0060 E-01 which is high at the customary 0.05 significance level and hence the null hypothesis was accepted, which implies that the characterization of κ using DCT based GGVF active contours was not very significant.

Comparison among the p-values of characterizations from GVF, GGVF and DCT based GGVF active contours shows that the p-values for GGVF active contour characterization was comparatively high while the p-values of GVF and DCT based GVF active contour characterization were very low; implying that the characterization results from GVF active contours and DCT based GVF active contours were highly significant.

Judged in conjunction with the graphical results, DCT based GVF active contours give better boundary mapping output with less number of indentations. Hence, it was established that DCT based GVF active contours was more efficient and performs better than its variants, namely, GVF, GGVF and DCT based GGVF active contours.

Therefore, the acceptable parameter range was determined from the characterization of DCT based GVF Active contours using the median as a tool for decision making. A 5% tolerance level was introduced to the acceptable parameter range to reduce the parameter range effects introduced by the characterization experimentation and to make it as an optimal parameter range that could be extended to similar classes of chromosome spread images.

Table 21: Optimal parameter range of DCT based GVF active contours for boundary mapping similar classes of chromosome spread images

Parameters	Acceptable parameter range	Acceptable parameter range at 5% tolerance
DCT GVF σ	0.2-0.5	0.1900-0.5250
DCT GVF μ	0.05-0.09375	0.0475-0.0984
DCT GVF α	0-0.125	0.0000-0.1313
DCT GVF β	0-0.5	0.0000-0.5250
DCT GVF κ	0.5-0.875	0.4750-0.9187

DCT based GVF active contours were used with this optimal parameter range for boundary mapping of chromosome spread images (Table 21). The very low error measures[16] establish that DCT based GVF active contours could also be used to accomplish good boundary mapping on similar classes of chromosome spread images using the same optimal range of parameter values.

CONCLUSIONS

The DCT based GVF active contours are hence established as a better and more efficient tool for boundary mapping of chromosome spread images compared to GVF active contours, GGVF active contours and DCT based GGVF active contours.

The optimal parameter range for DCT based GVF active contours obtained by characterization experiments can also be used for successful boundary mapping of similar classes of chromosome spread images using DCT based GVF active contours.

ACKNOWLEDGMENTS

The authors wish to thank Prof. Ken Castleman and Prof. Qiang Wu, both from Advanced Digital Imaging Research, Texas for their help in providing chromosome images.

REFERENCES

1. Britto, A.P. and G. Ravindran, 2005. Boundary mapping of chromosome images using gradient vector flow active contours and investigations. Acad. Open Internet J., http://www.acadjournal.com/2005/v15/part6/p6
2. Kass, M., A. Witkin and D. Terzopoulos, 1987. Snakes: Active contour models. Intl. J. Comp. Vision, 1: 321-331.

3. Rueckert, D., 1997. Segmentation and tracking in cardiovascular MR images using geometrically deformable models and templates. Ph.D Thesis, Imperial College of Science, Technology and Medicine, London, pp: 63-65.
4. Xu, C. and J.L. Prince, 1997. Gradient Vector Flow :A new external force for snakes, IEEE Proceedings of Conference on Comp. Vis. Patt. Recog. (CVPR'97), pp: 66-71
5. Leroy, B., I. Herlin and L.D. Cohen, 1996. Multi-resolution algorithms for active contour models. In: 12th Intl. Conf. Analysis and Optimization of Syst., pp: 58-65.
6. Cohen, L.D., 1991. On active contours and balloons. CVGIP: Image Understanding, 53: 211-218.
7. Cohen, L.D. and I. Cohen, 1993. Finite-element methods for active contour models and balloons for 2-D and 3-D images. IEEE Transactions On Pattern Anal. Machine Intell., 15: 1131-1147.
8. Davatzikos, C. and J.L. Prince, 1995. An active contour model for mapping the cortex. IEEE Transactions on Medical Imaging, 14: 65-80.
9. Davatzikos, C. and J.L. Prince, 1994. Convexity analysis of active contour models. In: Proc. Conf. Inform. Sci. Syst., pp: 581-587.
10. Abrantes, A.J. and J.S. Marques, 1996. A class of constrained clustering algorithms for object boundary extraction. IEEE Transactions on Image Processing, 5: 1507-1521.
11. Prince, J.L. and C. Xu, 1996. A new external force model for snakes. In 1996 Image and Multidimensional Signal Processing Workshop, pp: 30-31.
12. Xu, C. and J.L. Prince, 2000. Gradient Vector Flow Deformable Models. In: Handbook of Medical Imaging, Academic Press, pp: 159-170.
13. Xu, C. and J.L. Prince, 1998. Snakes, shapes and gradient vector flow. IEEE Transactions on Image Processing, 7: 359-369.
14. Xu, C. and J.L.Prince, 1998. Generalized gradient vector flow external forces for active contours. Signal Processing, 71: 131-139.
15. Tang, J. and S.T. Acton, 2004. A DCT based gradient vector flow snake for object boundary detection. 6th IEEE Southwest Symposium on Image Analysis and Interpretation, pp: 157-161.
16. Britto, A.P. and G. Ravindran, 2005. Boundary mapping of chromosome spread images using optimal set of parameter values. In: Discrete cosine transform based gradient vector flow active contours. J. Applied Sci., (Accepted).